

Evolution in the structural properties of early-type Brightest Cluster Galaxies at small lookback time and dependence on the environment

Mariangela Bernardi^{*}

Department of Physics & Astronomy, University of Pennsylvania, 209 S. 33rd St., Philadelphia, PA 19104, USA

30 October 2018

ABSTRACT

At the present time, early-type brightest cluster galaxies in the SDSS MaxBCG and C4 catalogs have larger sizes than early-type galaxies of similar luminosity, whether these other objects are in the field, or are satellites in clusters. BCG sizes are also stronger functions of luminosity $R_e \propto L$ than are the sizes of the bulk of the population; this remains true if one restricts attention to narrow bins in velocity dispersion. At fixed stellar mass *and* formation time, objects at lower redshift are larger and have smaller velocity dispersions – i.e. the sizes increase and velocity dispersions decrease with age. In addition, at any given redshift, younger BCGs have slightly larger sizes than older BCGs of the same stellar mass; however, they have similar velocity dispersions. As a result, at redshifts ~ 0.25 , corresponding to lookback times of order 3 Gyrs, BCGs are smaller than their lower redshift counterparts by as much as $\sim 70\%$ for the brightest BCGs: the sizes evolve as $(1+z)^{0.85(M_r+21)}$. Qualitatively similar but weaker evolution in the sizes is also seen in the bulk of the early-type population: at $M_r < -22$ the sizes evolve as $(1+z)^{0.7(M_r+21)}$, while at $M_r > -22$ the evolution is approximately $(1+z)^{-0.7}$, independent of M_r . The velocity dispersion–luminosity correlation also evolves: $(1+z)^{-0.2(M_r+21)}$ at $M_r < -22$ (as for the BCGs) and $(1+z)^{0.2}$ for fainter galaxies. The size– and velocity dispersion–stellar mass correlations yield consistent results, although, in this case, accounting for selection effects is less straightforward. These trends, in particular the fact that the velocity dispersions at fixed stellar mass decrease with age, are most easily understood if early-type BCGs grew from many dry minor mergers rather than a few major mergers. Only in such a scenario can BCGs be the descendents of the super-dense galaxies seen at $z \sim 2$; major dry mergers, which increase the size in proportion to the mass, cannot bring these galaxies onto the BCG $R_e - M_*$ relation at $z \sim 0$.

We also compared the ages and sizes of our early-type BCGs with other cluster galaxies (satellites). BCGs are larger than satellites of similar luminosity or stellar mass at the same redshift. Although both satellites and BCGs trace the same weak age– L or age– M_* relation, this can be understood by noting that BCGs are typically about 1 Gyr older than the satellites in their group, and they are about 0.5 mags more luminous. Finally, we find that the mean satellite luminosity is approximately independent of BCG luminosity, in agreement with recent predictions based on the luminosity-dependence of clustering.

Key words: galaxies: formation - galaxies: haloes - dark matter - large scale structure of the universe

1 INTRODUCTION

There has been recent interest in the sizes of galaxies: at fixed stellar mass, galaxies appear to be about a factor of

five smaller at $z \sim 2$ than at $z \sim 0$ (Trujillo et al. 2006; Cimatti et al. 2008; Van Dokkum et al. 2008; Younger et al. 2008; Buitrago et al. 2008; Tacconi et al. 2008; Chapman et al. 2008; van der Wel et al. 2008; Franx et al. 2008; Damen et al. 2008; Saracco et al. 2008). Similar evolution in the size–luminosity relation of radio galaxies was seen almost a

^{*} E-mail: bernardm@physics.upenn.edu

decade ago (Roche et al. 1998). This evolution is difficult to arrange in models where the galaxies form from a simple monolithic collapse.

On the other hand, qualitatively similar behaviour for dark matter halos has been expected for some thirty years: a virialized halo at a given epoch is approximately 200 times denser than the critical density at that epoch, whatever its mass (Gunn & Gott 1972). Thus, at fixed mass, the virial radius scales approximately as $(1+z)^{-1}$. Mass-independent densities appear to be a good description of cluster-mass halos locally (Abbas & Sheth 2007; Johnston et al. 2008; Vikhlinin et al. 2008) and at higher redshifts (e.g., Meneux et al. 2008). These halos are expected to have formed from essentially dissipationless mergers, so, for systems dominated by dissipationless merging, we expect that, at fixed mass, the radii are larger at late times.

One arrives at the same conclusion if one considers mergers along parabolic orbits (Ostriker & Hausman 1977; Ciotti 2008). For example, the velocity dispersion of the product of a parabolic merger of two equal mass galaxies is the same as that of its progenitors (this assumes mass and energy conservation). The virial theorem requires that if the mass has doubled with no change to the velocity dispersion, then the size must also have doubled, making the density smaller by a factor of four. This is the most extreme case: if the progenitor masses were unequal, then the density of the product is less than that of the more massive progenitor, but by a factor of less than four. Again, dissipationless mergers act to decrease the density.

Galaxy formation was not dissipationless (Fall & Efstathiou 1980; Barnes & Hernquist 1991): gas dissipation has played an important role, although this is expected to have been more true at high redshift (Hopkins et al. 2008). Subsequent major mergers between disk galaxies are thought to be the main way in which elliptical galaxies form (Toomre & Toomre 1972), possibly followed by dry dissipationless mergers in which both the size and the stellar mass of the final object increase. So, to answer the question of where, today, are the super-dense objects seen at high- z , it has been suggested that they must have undergone dissipationless mergers since then, so as to have gone unnoticed today. (Cimatti et al. 2008 note that there is a class of local objects which may be direct descendents of the high- z samples for which the merger hypothesis is unnecessary – these are the fast rotators in the sample of Bernardi et al. 2008 which have large σ but small sizes. But these objects are too rare to be the typical descendents. Recently, Trujillo et al. 2009 also found a very low number density of old superdense massive galaxies in the present Universe).

However, Fan et al. (2008) have shown a model which may be able to reproduce the observed evolution in the size- M_* relation. They assume that the AGN feedback which expels gas from the central regions produces a sudden reduction of mass in the core, as a result of which the stellar distribution puffs-up. In this model, the sizes increase, but the stellar masses do not. Since the peak of AGN activity was around $z \sim 2$, most of the size evolution in this model is over by $z \sim 1$. In contrast, dry mergers and evolution in hierarchical models is expected to continue to the present day.

One of the main goals of this paper is to study

the evolution in the sizes of objects for which dry dissipationless merging is thought to have been most common – early-type BCGs (Malumuth & Kirshner 1981; Malumuth & Kirshner 1985; Oegerle & Hoessel 1991; Lauer et al. 2007; Bernardi et al. 2007; Tran et al. 2008). BCGs at $0.4 < z < 1$ have been compared with more local samples recently. One study concludes that the stellar mass appears to not have grown significantly since $z \sim 1$ (Whiley et al. 2008), but does not include a study of the BCG sizes. Another suggests that the sizes may have been smaller at high redshift, but some of this apparent evolution was almost certainly a consequence of not looking at fixed restframe wavelength or stellar mass (Nelson et al. 2002).

Section 2 describes our early-type BCG sample in which we have size, stellar mass and age estimates out to $z \sim 0.3$. In Section 3 we show that, at fixed (evolution corrected) luminosity BCGs were larger in the past, and they had smaller velocity dispersions. This remains true if we replace luminosity with stellar mass, although in this case the measurement is complicated by selection effects (as we illustrate in Appendix A, where we also discuss how correlated errors in stellar mass and age can compromise the observed correlations). We also show that the objects which formed earlier are smaller, but their velocity dispersions are not larger – whereas the former is expected in monolithic collapse models the latter is harder to arrange.

In Section 4 we compare the sizes and ages of BCGs to those of other cluster galaxies. This complements recent work indicating that non-central or satellite luminosities should be approximately independent of the mass of a group or the luminosity of the central BCG (Skibba et al. 2006; Skibba et al. 2007).

A final section summarizes our results. Appendix B discusses how our luminosity-size correlation for BCGs compares with other recent determinations.

Complementary studies of the sizes and velocity dispersion of the bulk of the local early type population are presented in Shankar & Bernardi (2009) and Shankar et al. (2009). These other studies show that the size-luminosity relation of galaxies with $L_r < 10^{11} L_\odot$ at $z \sim 0$ is independent of the age of the stellar population, implying that the size-stellar mass relation does depend on age: older galaxies are smaller than younger galaxies of the same stellar mass. However, they find a weak dependence of the velocity dispersions (at fixed mass) on galaxy age – this is difficult to accommodate in a monolithic-based collapse model. The amplitude of these trends for massive galaxies ($L_r > 10^{11} L_\odot$) is even smaller.

As discussed below, we show that BCGs/massive galaxies are different from the bulk of early-type galaxies; their properties are more consistent with formation from predominantly dissipationless mergers than from a monolithic collapse.

2 THE SAMPLE

We would like to study early-type BCGs over a relatively large range in redshift. Since we are most interested in evolution, we would like the sample to be homogeneously selected over the entire redshift range. This motivates the use of the **MaxBCG** catalog which was assembled by Koester et al.

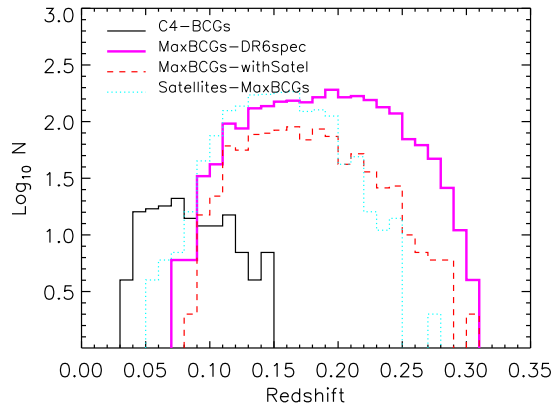


Figure 1. Redshift distribution of BCGs from the C4 (thin solid) and MaxBCG (thick solid) catalogs. Dot-dashed histogram shows the redshift distribution of the objects we identify as satellites, and dashed histogram shows the redshift distribution of the subset of BCGs which host these satellites.

(2007) from the SDSS. It spans the range $0.07 < z < 0.3$; the 13823 groups and clusters in it each contain at least 10 galaxies brighter than $0.4L_*$ in the r -band (i.e., brighter than about -19.5 mags in r).

At the very least, we would like to study BCG luminosities and sizes over this redshift range, but, if possible, we would like to study velocity dispersions and stellar masses as well. Of 13823 clusters in the MaxBCG catalog, 5413 are reported to have BCGs with spectroscopic redshifts. However, upon matching with the SDSS-DR6 (Adelman-McCarthy et al. 2008), we find 7832 objects with spectroscopic redshifts. A subset of 4912 has deVaucouleur apparent magnitude between 14.5 and 17.5. Requiring $\text{fracDev} > 0.8$ in both the g - and r -bands is a good way to select early-types; this reduces the sample size to 4350. Of these, 2634 have stellar mass estimates from Gallazzi et al. (2005), and only 2012 of these have estimated velocity dispersions. For the objects with stellar mass estimates, Gallazzi et al. (2005) also provide (luminosity weighted) age estimates. The results which follow that are based on L rather than M_* do not depend on whether or not we used 4350 or 2634 galaxies. (Requiring that velocity dispersions were estimated but not caring about M_* makes the sample size 3277.)

We will also be interested in how BCGs compare to non-central or satellite galaxies. We do this in two ways. First, we search an appropriately chosen volume around each MaxBCG in our sample as follows. The catalog contains an estimate of the number of galaxies, N_{gal} in the group associated with each BCG. We define a velocity dispersion $\sigma_{\text{group}} \equiv 100 \sqrt{1.33 N_{\text{gal}}} \text{ km s}^{-1}$ and a radius $r_{\text{group}} \equiv \sigma_{\text{group}}/7/70 \text{ Mpc}$. The scaling between group velocity dispersion and N_{gal} is close to that reported by Becker et al. (2007) in their analysis of this catalog. The relation between group radius and velocity dispersion is chosen to approximately match the expected scaling for dark matter halos. We identify as satellites all objects which are within r_{group} across and $2\sigma_{\text{group}}$ along the line of sight to a BCG in the catalog. Having identified the satellites, we would now like to exclude those that are of later type. We do so by

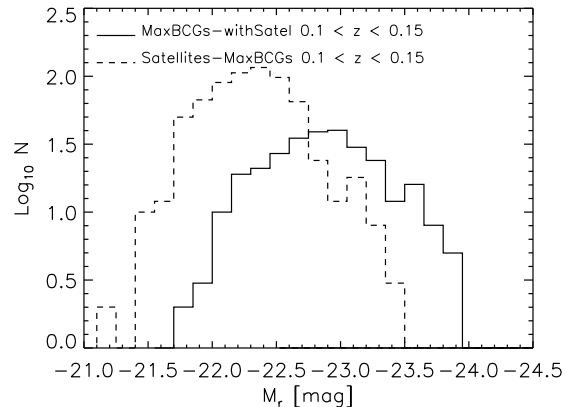


Figure 2. Luminosity distribution of early-type MaxBCGs with early-type satellites (solid), and satellites (dashed) over the range $0.1 < z < 0.15$.

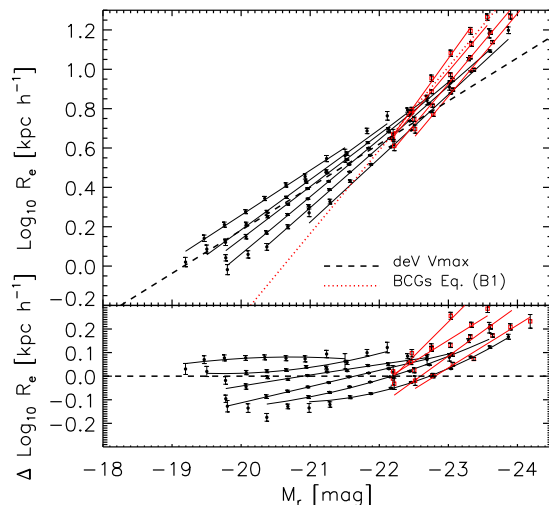


Figure 3. Size-luminosity relation for the bulk of the population (dashed) and BCGs (dot-dashed). Filled symbols show this relation when the sample is restricted to a narrow range in σ : results for 6 bins of width 0.1 dex, starting from $\log_{10} \sigma = 1.9$, are shown. Open circles show a similar analysis of the BCGs: 4 bins of width 0.05 dex, starting from $\log_{10} \sigma = 2.3$.

applying the same selection cuts as we did to identify early-type BCGs. This leaves a sample of 1734 objects – less than half the full sample of satellites.

Note that our satellite sample is smaller than the BCG sample; this might seem in conflict with our previous statement that each maxBCG cluster has at least 10 satellites brighter than $0.4L_*$. This is because we are requiring that satellites have measured spectra; because of the SDSS magnitude limit, spectra of $0.4L_*$ objects are not available beyond $z \sim 0.05$. For example, of the 1734 satellites in our sample, 1555 have $M_r < -22$. Thus, the vast majority of these objects are more luminous than $3L_*$ – they represent the bright-end of the satellite luminosity function. In addition, if an SDSS fiber was placed on a BCG, then objects within 55 arcsecs of it will not have an SDSS spectrum. These fiber-collisions affect a larger physical scale for the higher redshift

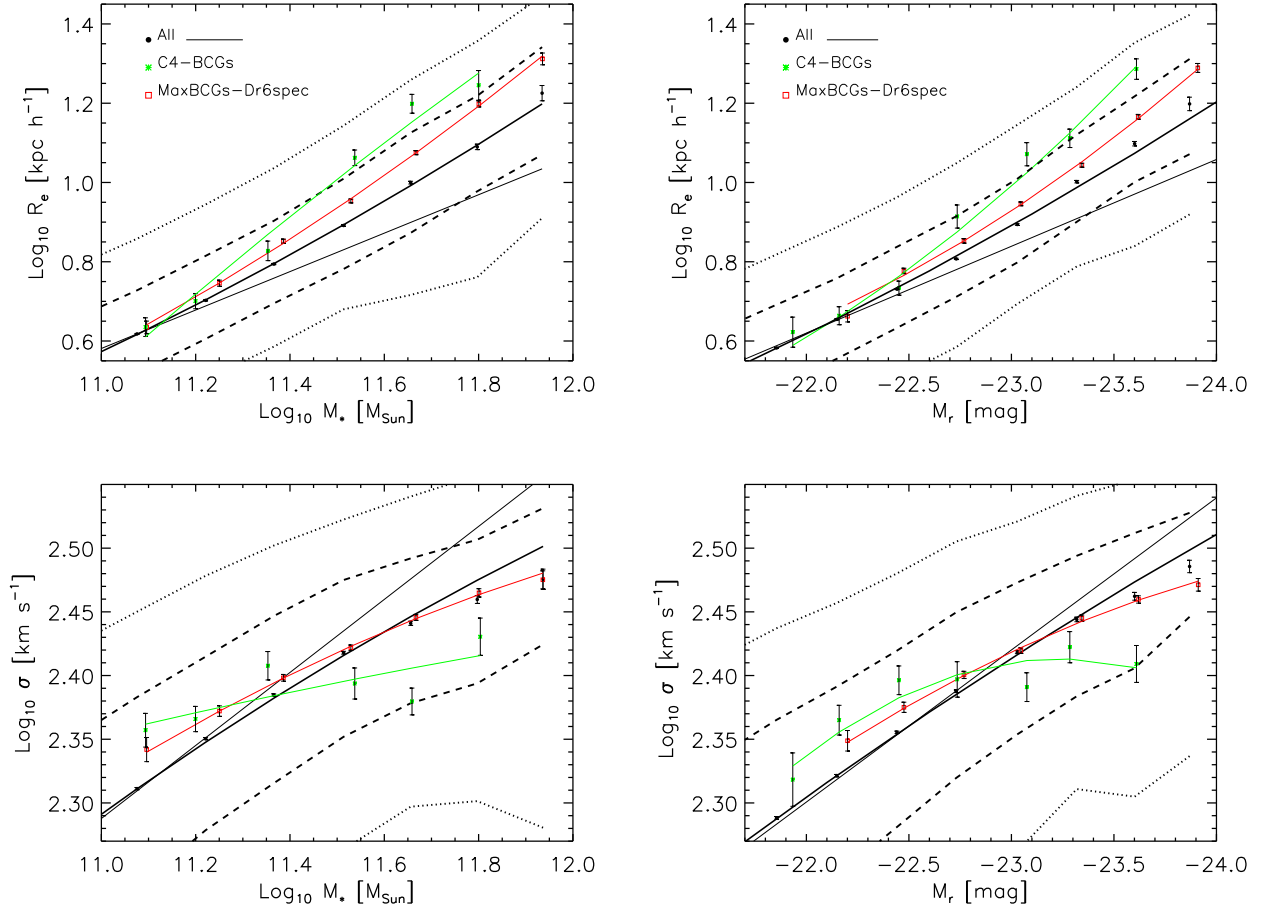


Figure 4. Size-luminosity and stellar mass relations for BCGs in the C4 and MaxBCG samples, and for the bulk of the early-type population (top), and similarly when size is replaced by velocity dispersion (bottom). At fixed L or M_* , the C4 BCGs are larger than MaxBCGs, and both are larger than the mean relation traced by the bulk of the population. The objects with largest sizes have the smallest velocity dispersions.

clusters, further reducing the number of satellites with measured spectra.

At lower redshifts, we use the C4 catalog of Miller et al. (2005). Although this is a rather different catalog, we show below that if we extrapolate the trends we see in the MaxBCG catalog to smaller z , then they are in good agreement with those in the C4 catalog. Furthermore, there is previous work on the C4 BCG catalog; studying this catalog allows us to tie our measurements to those in the literature (see Appendix B). This is important because, although all the objects we analyze are drawn from the SDSS database, the photometric quantities (magnitudes, half-light radii) are not exactly the same as those output by the survey. Rather, we use the prescriptions in Hyde & Bernardi (2009) to correct the SDSS parameters for known sky subtraction problems with the photometry of bright objects in crowded fields.

Figure 1 shows the distribution of early-type BCG redshifts in the C4 (solid) and MaxBCG (MaxBCG-DR6spec, solid) catalogs (the C4 BCGs probe lower redshifts), the redshift distribution of MaxBCG early-type satellites (dotted), and the redshift distribution of early-type MaxBCGs with early-type satellites (MaxBCG-withSatel, dashed). The satellite distribution does not extend to as high redshifts, be-

cause satellites are fainter than BCGs (by definition). The dashed histogram shows the redshift distribution of those BCGs which have satellites with spectroscopic information. Most of the high redshift BCGs have no satellites, due to the combined effects of the magnitude limit and fiber-collisions. However, over the redshift range $0.1 < z < 0.15$ there are approximately three satellites per BCG; we will only use the objects in this range when we compare BCG and satellite properties. Figure 2 shows the distribution of (evolution corrected) luminosities over this range: the mean BCG luminosity is about half a magnitude brighter.

3 THE SIZE-LUMINOSITY AND SIZE-STELLAR MASS RELATIONS

The main goal of this section is to present measurements of the correlation between (restframe) size and (evolution corrected) luminosity in a few redshift bins. (The measured luminosities are corrected for known problems associated with the SDSS sky subtraction algorithm following Equation 2 in Hyde & Bernardi 2009. They are then corrected for evolution, by adding $0.9z$ to all absolute magnitudes.

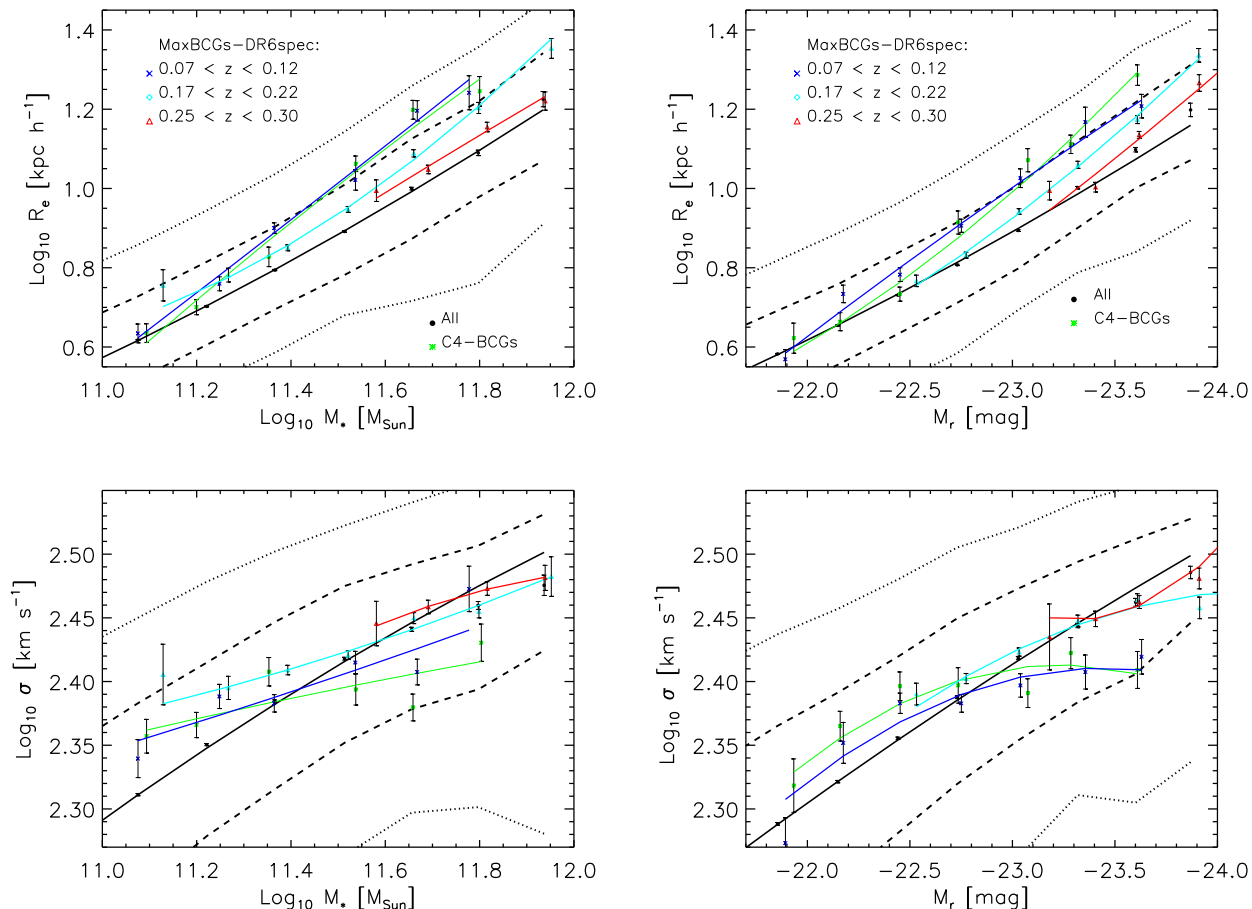


Figure 5. Same as previous figure, but now for objects from the MaxBCG sample only, subdivided into redshift bins as indicated. At fixed luminosity or stellar mass, the BCGs in the lowest redshift bin are larger and have smaller velocity dispersions.

The sizes are corrected for the known sky subtraction problems and for the fact that early-type sizes depend on wavelength following Equations 3 and 6 in Hyde & Bernardi 2009, respectively.) Inferences about evolution in this correlation depend upon how much one believes that the effects of luminosity evolution have been removed. For this reason, one might have thought it preferable to study the correlation between size and stellar mass. In what follows, we will show these relations side-by-side, but emphasize that because the SDSS is magnitude limited, evolution in correlations with M_* should be interpreted carefully. Appendix A discusses why. Appendix B compares the BCG size-luminosity relation we find here with other determinations in the recent literature.

Note that although our M_* estimates are from Gallazi et al. (2005), we correct them slightly to account for the fact that they actually come from multiplying an estimate of M_*/L by the observed luminosity. The L used by Gallazi et al. did not account for the SDSS sky subtraction problem, so we divide their M_* estimates by the same correction factor we used for the magnitudes (Equation 4 in Hyde & Bernardi 2009).

3.1 Abnormally large sizes

The sizes and luminosities of early-type galaxies are correlated: the mean size increases with luminosity as $R \propto L^{0.6}$ (e.g. Hyde & Bernardi 2009). However, BCGs follow a steeper relation: $R \propto L$ (see Appendix B), and it has long been argued that this is evidence for formation histories that are dominated by dry mergers. The argument is not so straightforward, however. This is because objects with small values of σ are not BCGs, so BCGs have a narrower distribution in σ than the bulk of the population. However, for the bulk of the population, the $R - L$ correlation at fixed σ is considerably steeper, $R \propto L^{0.9}$, than when averaged over all σ (Bernardi et al. 2003; Bernardi et al. 2008). So one may ask if the steeper relation for BCGs can be attributed to the fact that they are biased to larger σ .

Figure 3 presents a direct comparison: the dashed and dot-dashed lines in the top panel show the $R_e - L$ relation for the bulk and for the early-type BCGs, and the various solid lines show this relation for narrow bins in σ : the lines are offset to smaller R_e as σ increases. The bottom panel shows these relations after subtracting-off the dashed line. This shows clearly that, except for the smallest bin in σ , the other relations are all steeper. However, the BCGs are steeper still: the $R_e - L$ relation of BCGs is steeper than

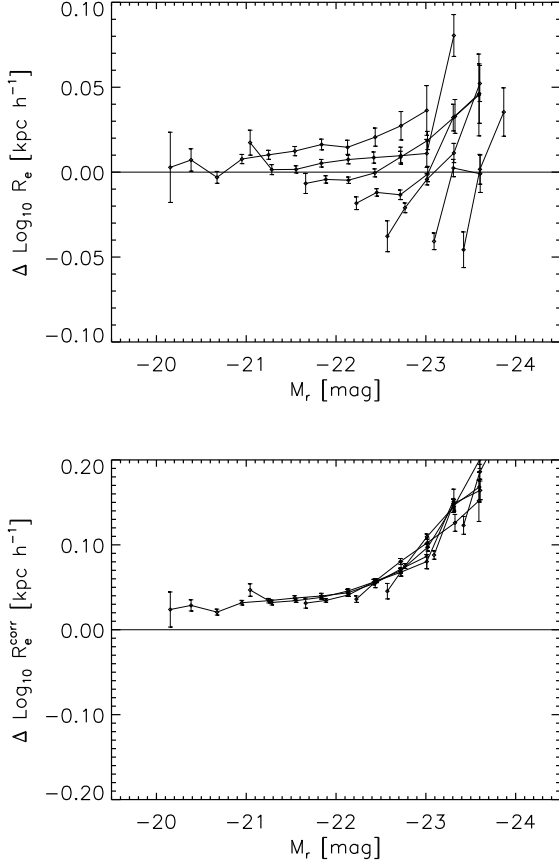


Figure 6. Residuals from the size-luminosity relation $\Delta \log_{10} R_e \equiv \log_{10}(R_e/\text{kpc}) - (4.72 + 0.63 M_r + 0.02 M_r^2)$, for the bulk of the early-type galaxy population in different redshift bins: $0.07 < z \leq 0.1$, $0.1 < z \leq 0.13$, $0.13 < z \leq 0.16$, $0.16 < z \leq 0.19$, $0.19 < z \leq 0.22$, $0.22 < z \leq 0.25$ and $z > 0.25$. At $M_r > -22$, there is a tendency for the objects at higher redshift to have slightly smaller σ . At $M_r < -22$, the difference in size between two different redshift bins increases for brighter galaxies, in agreement with the evolution seen for BCGs in Figure 5. Bottom panel shows the result of applying the corrections in Equations 1 and 3.

that of the bulk, even at fixed σ . In the next subsections, we study other evidence that BCGs are a different population.

3.2 Evidence for evolution

The top panels in Figure 4 compare the size-luminosity and stellar mass relations for the BCGs in the C4 and MaxBCG catalogs, with the relations traced out by the bulk of the early-type galaxy population. At fixed L , the C4 BCGs are larger than MaxBCGs, and both are larger than the mean relation traced by the bulk of the population. These differences are most pronounced for the most luminous objects; there is essentially no effect at $M_r > -22.5$ or $\log_{10}(M_*/M_\odot) < 11.2$.

The bottom panels show that complementary differences are seen when size is replaced with velocity dispersion: at the brightest luminosities ($M_r < -23$) C4 BCGs have the smallest velocity dispersions. While the trends at the bright

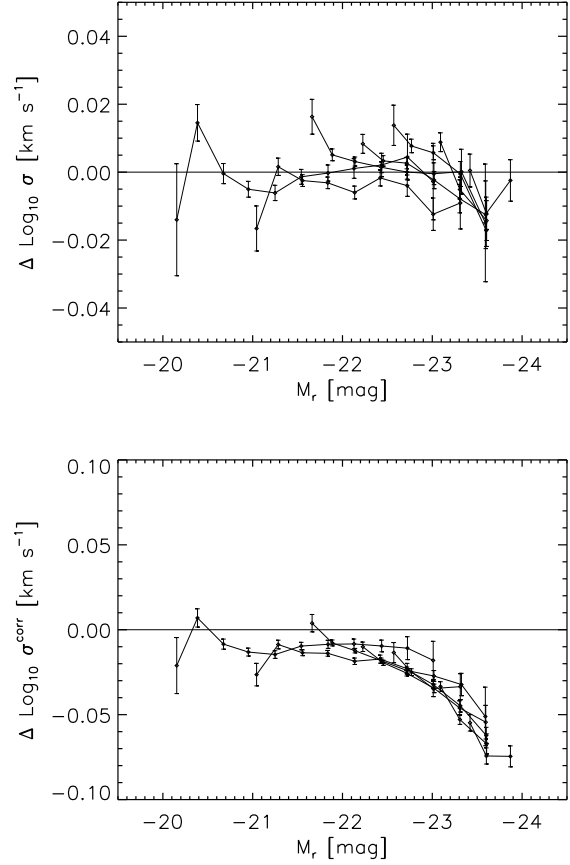


Figure 7. Same as the previous figure, but now for the σ -luminosity relation: $\Delta \log_{10} \sigma \equiv \log_{10}(\sigma/\text{kms}^{-1}) - (-2.97 - 0.37 M_r - 0.006 M_r^2)$, for the bulk of the early-type galaxy population in different redshift bins. Bottom panel shows the result of applying the corrections in Equations 2 and 4.

end are the ones of most interest in the present context, we note that, at fainter luminosities, BCGs tend to have larger σ for their L than the bulk of the population.

That BCGs have larger sizes and smaller velocity dispersions than the bulk is no surprise – what *is* surprising is the significant difference between the two BCG samples. Although it is possible that this is related to the fact that the two samples span different redshift ranges, it is also possible that systematic differences between how the catalogs were assembled are to blame.

To eliminate the second possibility, Figure 5 shows a similar analysis, but now restricted to MaxBCG objects only. Since this sample is relatively large, we divided it into subsamples in redshift: $0.07 < z < 0.12$, $0.17 < z < 0.22$ and $0.25 < z < 0.30$. This shows clearly that, even within the MaxBCG catalog itself, the lower redshift BCGs tend to have larger sizes and smaller velocity dispersions than their higher redshift counterparts of similar luminosity or stellar mass. Moreover, the MaxBCGs in the lowest redshift bin tend to follow similar scaling relations to those defined by the C4 BCGs.

Finally, Figure 6 shows the $R_e - L$ relation for the bulk of the early-type galaxy population. (Recall that the measured luminosities have been corrected for evolution

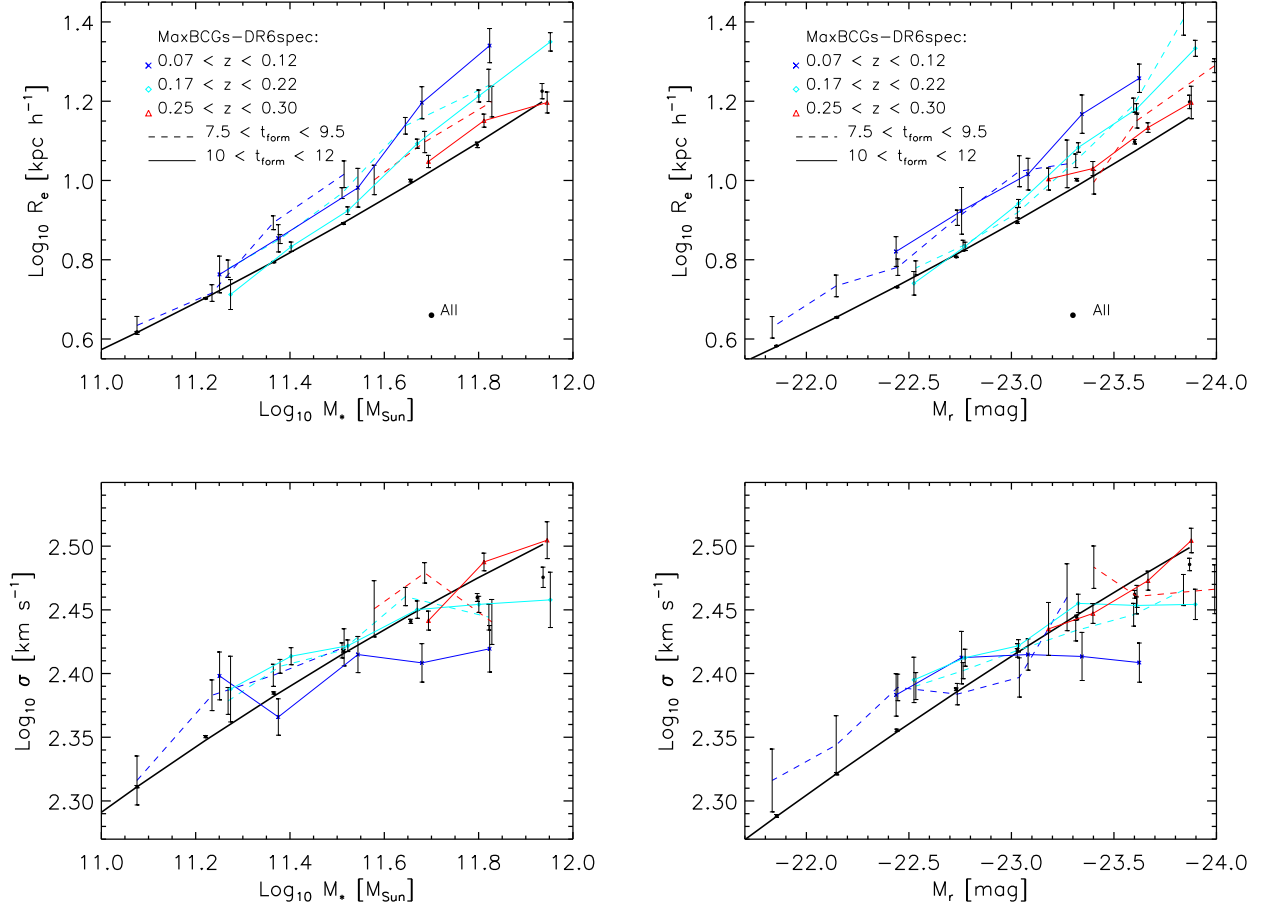


Figure 8. Same as Figure 5, but now the objects in each redshift bin are subdivided by the lookback time to when their stars formed. At fixed formation time, objects at low redshift have larger sizes and smaller velocity dispersions than their higher redshift counterparts of similar M_* (left) or L (right).

by adding $0.9z$ to all absolute magnitudes, and the sizes are corrected for the fact that early-type sizes depend on wavelength.) Each set of symbols shows data from a number of redshift bins: $0.07 < z \leq 0.1$, $0.1 < z \leq 0.13$, $0.13 < z \leq 0.16$, $0.16 < z \leq 0.19$, $0.19 < z \leq 0.22$, $0.22 < z \leq 0.25$ and $z > 0.25$. To reduce the range of sizes, in the top panel we have subtracted out a fiducial relation to better see if there is any evolution: we actually show $\Delta \log_{10} R_e \equiv \log_{10}(R_e/\text{kpc}) - (4.72 + 0.63 M_r + 0.02 M_r^2)$ (from Table 1 of Hyde & Bernardi 2009). The top panel in Figure 7 shows a similar analysis of the velocity dispersions, for which $\Delta \log_{10} \sigma \equiv \log_{10}(\sigma/\text{kms}^{-1}) - (-2.97 - 0.37 M_r - 0.006 M_r^2)$ (from Table 1 of Hyde & Bernardi 2009).

There is a hint that the higher redshift objects have smaller sizes. At $M_r < -22$, the difference in size between two different redshift bins increases for brighter galaxies, in agreement with the evolution seen for BCGs (Figure 5). At the bright end ($M_r < -22$), we find that the evolution depends on the luminosity of the galaxy: the sizes evolve as $(1+z)^{0.7(M_r+21)}$ and the velocity dispersions as $(1+z)^{-0.2(M_r+21)}$. At fainter luminosities ($M_r > -22$), the evolution is weaker; we approximate it as $(1+z)^{-0.7}$ and $(1+z)^{0.2}$. Hence, to correct the sizes and velocity disper-

sions to $z = 0$ one could use:

$$\log_{10} \left(\frac{R_e^{\text{corr}}}{\text{kpc}} \right) = \log_{10} \left(\frac{R_e}{\text{kpc}} \right) - 0.7(M_r + 21) \log(1+z) \quad (1)$$

$$\log_{10} \left(\frac{\sigma^{\text{corr}}}{\text{kms}^{-1}} \right) = \log_{10} \left(\frac{\sigma}{\text{kms}^{-1}} \right) + 0.2(M_r + 21) \log(1+z) \quad (2)$$

if $M_r < -22$ and by

$$\log_{10} \left(\frac{R_e^{\text{corr}}}{\text{kpc}} \right) = \log_{10} \left(\frac{R_e}{\text{kpc}} \right) + 0.7 \log(1+z) \quad (3)$$

$$\log_{10} \left(\frac{\sigma^{\text{corr}}}{\text{kms}^{-1}} \right) = \log_{10} \left(\frac{\sigma}{\text{kms}^{-1}} \right) - 0.2 \log(1+z) \quad (4)$$

if $M_r > -22$. The bottom panels in the two figures show the result of applying these corrections. We show below that the scaling at the bright end is slightly smaller than the luminosity dependent evolution in the sizes of our BCG sample which goes as $(1+z)^{0.85(M_r+21)}$.

3.3 Dependence on age and formation time

If we are seeing evolution, then it is interesting to ask if this depends on the age or formation time of the stellar population. E.g., the simplest monolithic collapse models predict

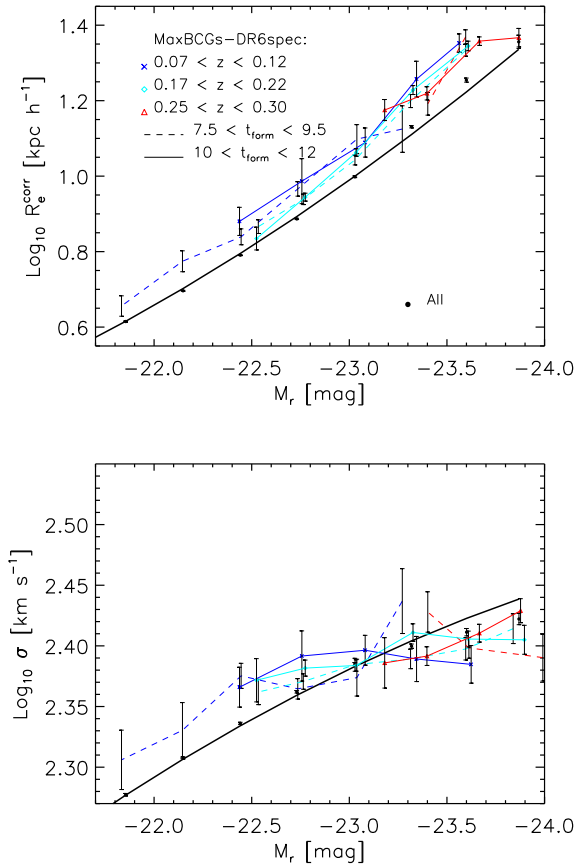


Figure 9. Same as right-hand panels of previous figure, but now after correcting the sizes and velocity dispersions for evolution using Equations 1 and 2.

that, for fixed formation time, there should otherwise be no dependence on age. To address this, we use age estimates of the stellar populations in these galaxies (from Gallazzi et al. 2005); these, with the observed redshifts, yield the lookback time to when the stars formed. (Because the age and M_* estimates have significant uncertainties, and they are correlated, it is important to use ages that are output from the same models which estimate M_* .)

Figure 8 is similar to Figure 5, but now the objects in each redshift bin have been divided into two subgroups, based on the formation time of the stars. These two bins correspond approximately to $z_{\text{form}} \sim 2.5$ (solid lines) and 1.25 (dashed lines).

We begin with a comparison of the solid lines in the panels on the left. These show that, for fixed formation time, older objects have larger sizes (top left) and smaller velocity dispersions (bottom left) than younger objects of the same stellar mass. The same is true of the dashed lines in these panels: size increases and velocity dispersion decreases as the galaxy population ages. The increase in size is more easily accommodated in dry merger models, and the decrease in velocity dispersion suggests that these mergers were minor.

Comparison of the dashed and solid curves for a given redshift of observation shows that, for a given stellar mass, the objects which formed more recently have larger sizes.

While this is qualitatively consistent with having formed when the Universe was less dense, the difference is much less than the factor of $\log_{10}(3.5/2.25) = 0.2$ dex one might naively have expected. Similarly, the velocity dispersions of the objects which formed more recently are not much smaller than when the formation redshift was higher. Presumably, this is because the sizes of the older objects have increased from their initial values, and the velocity dispersions have decreased (as suggested by comparing the solid lines with one another, and the dashed lines with one another).

There are important qualitative differences when one uses luminosity rather than M_* , meaning that care must be taken when translating trends seen in plots with L into trends with M_* . The top right panel shows that, at a given redshift of observation, the size-luminosity correlation does not depend on formation time (solid and dashed lines overlap), and the $\sigma - L$ relation does not either (bottom right panel). This may be understood as follows. The panel on the right is obtained by shifting each galaxy in the panel on the left by its $(M_*/L)^{-1}$. In a model where the stars age passively (whatever the assembly history), the older population has a larger M_*/L : the expected difference in M_*/L between the two age bins is about 0.1 dex ($M_*/L \propto t^{0.75}$ or so, where t is the age of the population). So, if we start from the $R_e - M_*$ relation, then the solid curves in each redshift bin should shift towards the left, bringing them closer to the dashed ones.

Finally, Figure 9 shows the effect of correcting the sizes and velocity dispersions of our early-type BCGs using an equation similar to Equation (1) (since the size evolution of BCGs is better described by $(1+z)^{0.85(M_r+21)}$ we replace 0.7 with 0.85) and Equation (2). These corrections bring the curves associated with different redshifts into better agreement, suggesting that they have captured most of the evolution.

We conclude that, at fixed luminosity or stellar mass, the high redshift BCGs are denser, with the effect being more pronounced for objects with the largest luminosities or stellar masses. The most straightforward interpretation of this observation is that *the sizes and velocity dispersions of luminous BCGs are evolving in a manner which is qualitatively consistent with assembly histories that are dominated by dissipationless mergers which are still happening at low redshift*; the large size of our sample has allowed a detection of this even though it spans only a small lookback time.

Before we conclude this section, we emphasize again that one must be cautious when replacing luminosity with stellar mass, since selection effects can complicate the measurement (as we illustrate in Appendix A). Working with age and M_* presents additional complications because errors in age and M_*/L are correlated (see Appendix A2 for further discussion).

4 CENTRALS AND SATELLITES

Early-type BCGs tend to have larger sizes than the bulk of the early-type galaxy population. So one might wonder if the large sizes of BCGs are something that is characteristic of the group/cluster environment, or if this is specific to BCGs.

To address this, Figure 10 compares the scaling relations of the objects we identified as early-type satellites,

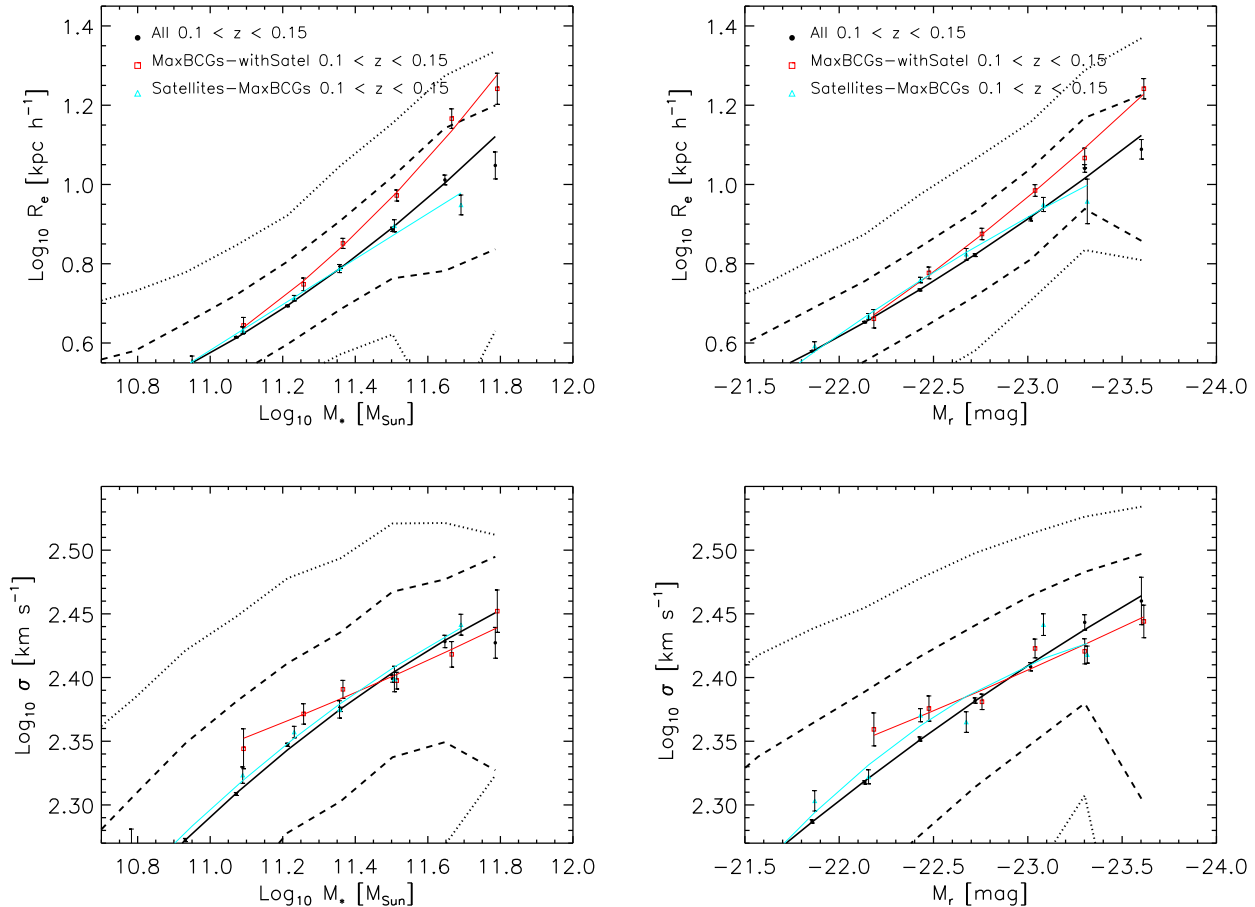


Figure 10. Comparison of sizes and velocity dispersions of BCGs and non-central/satellite cluster galaxies of similar luminosity and stellar mass, in a narrow redshift bin.

with those for early-type BCGs and for the bulk of the early-type population. This comparison indicates that the non-central/satellite early-types tend to be very similar to the bulk of the early-type population; it is the BCGs which are different. At $\log_{10}(M_*/M_\odot) > 11.4$ they have unusually large sizes with the effect increasing at large M_* ; at lower masses ($\log_{10}(M_*/M_\odot) < 11.4$), there is a hint that BCG velocity dispersions are larger than those of satellites and of the bulk of the early-type population (a hint also seen in Figure 5).

Our findings appear to contradict those of Weinmann et al. (2008), who report that the sizes of early-type central galaxies are *not* larger than the sizes of early-type satellites of the same stellar mass (see their Fig. 4). In part the difference is due to the fact that they studied groups which are less massive than ours. In addition, we suspect that some discrepancy could also arise because they use Petrosian-based quantities which are ill-suited for this sort of analysis (Hyde & Bernardi 2009).

The ratio of dynamical to stellar mass is another quantity of recent interest (Hyde & Bernardi 2009); it increases at large masses, suggesting that star formation is inefficient at large mass. Figure 11 shows that this ratio is about 0.05 dex larger for BCGs than it is for the bulk of the pop-

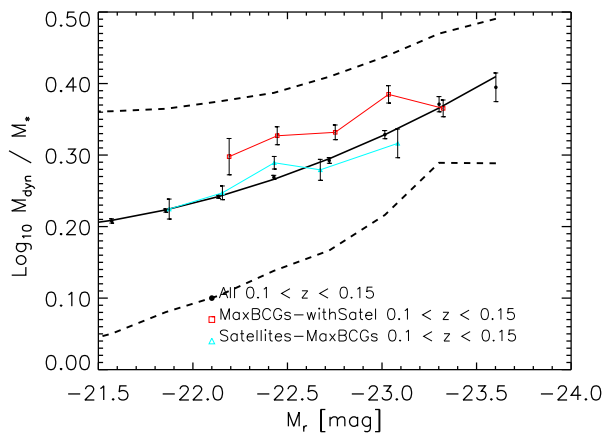


Figure 11. The dynamical to stellar mass ratio versus absolute magnitude of BCGs and non-central/satellite cluster galaxies of similar luminosity and stellar mass, in a narrow redshift bin.

ulation of the same luminosity, whereas the satellites are similar to the bulk of the population. At the bright end ($M_r < -22.8$), the difference is primarily due to the differ-

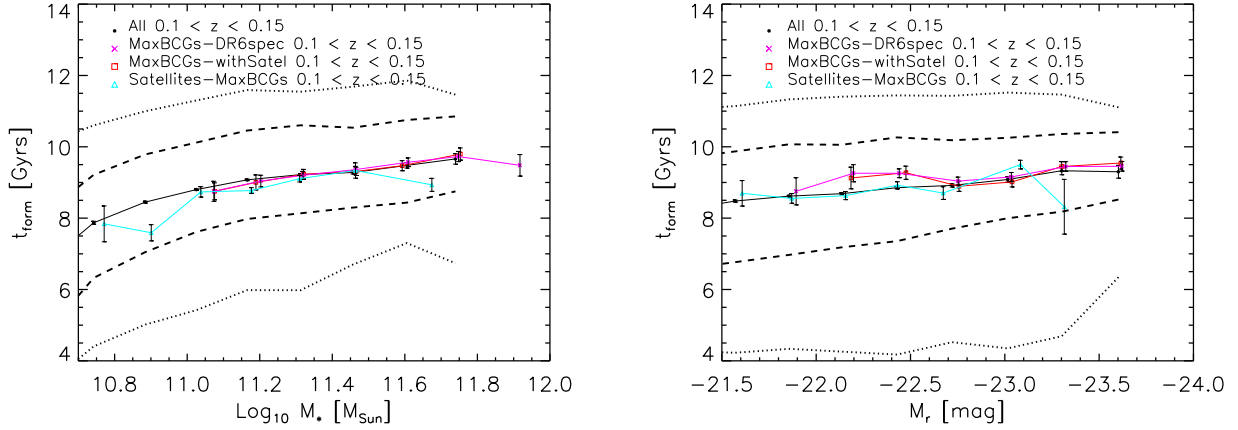


Figure 12. Correlation between lookback time to formation and stellar mass (left) or luminosity (right) for BCGs (squares) and satellites (triangles), over the redshift range where the number counts differ by a factor of about 3. Filled circles show the locus traced by the bulk of the early-type population; dashed and dotted lines show the region containing 68% and 95% of the objects.

ences in sizes – the velocity dispersions of BCGs are similar to those of satellites of the same luminosity. In a model where BCGs formed from dissipationless mergers this is easily understood: the offset to large M_{dyn}/M_* is associated not with lower star formation efficiency, but with the subsequent assembly of the stars which has increased the sizes more than the velocity dispersions. At the faint end ($M_r > -22.5$), the difference is probably due to the velocity dispersions rather than to the stellar masses.

We have also studied the correlation between the ages and luminosities or stellar masses of BCGs and satellites. (Appendix A discusses why, at smaller M_* than we show here, the trends with stellar mass may be strongly affected by selection effects – see Figure A3.) Figure 12 shows that at luminosities of about L_* (i.e., ~ -21.2 mag in the r -band) and larger, the bulk of the population defines an age- M_* or age- L relation: massive or more luminous galaxies tend to be slightly older. There is a hint that, about a magnitude brighter than L_* , BCGs are slightly older (~ 0.5 Gyr) than other objects of the same luminosity; but there is no difference at brighter or fainter L , and there is no difference when compared with objects of the same M_* . Satellites and BCGs (whether or not they have satellites) follow the same age- M_* relation as the bulk of the population. This is remarkable, given that we see this trend over a redshift range where the counts of centrals and satellites are approximately proportional to one another (Figure 1). Given that the BCGs in the same volume are more luminous (Figure 2), and have larger stellar masses on average, one might have expected the BCGs to also be older. Our results indicate that, if they have the same stellar mass, satellites and BCGs have the same age.

To understand why this happens, we now compare the luminosity-weighted age difference between satellites and their BCG, as a function of BCG luminosity. Figure 13 shows that BCGs tend to be older than their satellites, by about 0.5 – 1 Gyrs, over about two magnitudes in BCG luminosity – a range over which the mean BCG age changes by about 1 Gyr. (Our results are unchanged if we use the number- rather than luminosity-weighted age difference.)

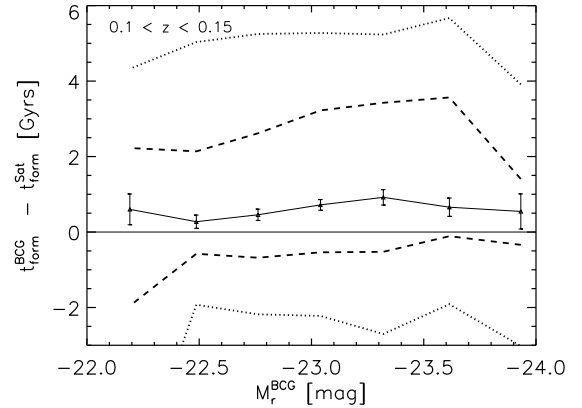


Figure 13. Difference between the mean luminosity-weighted age of the satellites in a group, and that of the BCG, as a function of BCG luminosity.

The younger ages with the smaller luminosities conspire to keep the satellites and BCGs along the same age- L or age- M_* relations.

5 DISCUSSION

Early-type BCGs have larger sizes than other early-type galaxies of similar luminosity or stellar mass. If restricted to a narrow bin in velocity dispersion, the size- L relation of the bulk of the population is steeper, suggesting that perhaps it is the fact that BCGs are biased towards larger velocity dispersions that is the origin of this difference. However, at fixed σ , the BCG $R_e - L$ scaling relation is steeper still (Figure 3).

Moreover, the sizes of BCGs appear to be evolving: higher redshift BCGs had smaller sizes than their local counterparts of the same (evolution corrected) luminosity or stellar mass (Figure 5). The evolution in the $R_e - L$ relation of the early-type BCG population is more evident (and in gen-

eral of galaxies with $\sim M_r < -22$) than that of the bulk of the early-type population at fainter luminosity: the BCGs sizes evolve as $(1+z)^{0.85(M_r+21)}$ (Figures 9). For the bulk of the early-type population, at the bright end ($M_r < -22$) the sizes evolve as $(1+z)^{0.7(M_r+21)}$ and the velocity dispersions (as for BCGs) as $(1+z)^{-0.2(M_r+21)}$ (Figures 6 and 7). At fainter luminosities ($M_r > -22$), the evolution is weaker; it goes as $(1+z)^{-0.7}$ and $(1+z)^{0.2}$. See Shankar & Bernardi (2009) for a more detailed analysis of the bulk of the population, who conclude that the more massive galaxies ($L_r > 10^{11} L_\odot$) show stronger evidence of the effects of dissipationless mergers.

The cleanest tests of the evolution we see come from restricting the BCG sample to narrow bins in formation time. At fixed formation time and stellar mass, the objects observed at lower redshift are larger, and their velocity dispersions are smaller (compare solid curves in Figure 8). The evolution, which we detect over lookback times as small as 1 Gyr, is difficult to reconcile with the simplest monolithic collapse models, and is most pronounced for the most luminous objects. The recent growth in BCG sizes is in qualitative agreement with hierarchical galaxy formation models in which the assembly of BCGs continues to the present day (De Lucia et al. 2006; Almeida et al. 2007).

Figure 8 also shows that the objects which formed earlier are smaller, but their velocity dispersions are not larger (compare dashed with solid curves in Figure 8). Whereas the former is expected in the simplest monolithic collapse models – the universe was denser at high redshift, so one expects the younger objects of a given mass to be smaller and have larger velocity dispersions – the latter is harder to arrange. Thus, both trends in Figure 8 – the evolution of the sizes and velocity dispersions of objects (of fixed stellar mass) that formed at the same time, and the dependence of the sizes and velocity dispersions on formation time – are difficult to accommodate in the simplest monolithic collapse models.

Recently, Fan et al. (2008) have suggested a *puffing-up* scenario for the evolution in the size– M_* relation — it postulates that it is the sizes which evolve, not the stellar masses. This model exploits the fact that the superdense galaxies mentioned in the Introduction are observed at about the epoch at which QSOs are most active; feedback from the AGN activity at $z \sim 2$ or 3 is assumed to expel gas from the central regions. The sudden reduction of mass in the core makes the surrounding stellar distribution puff up, after which the objects settle down to new (larger) sizes. *This is expected to have been completed by $z \sim 1$, whereas our observations of evolving sizes are at low redshift, so it seems unlikely that this mechanism can explain our measurements.* Also, there is little evidence for recently outflowing gas in our BCG sample. Nevertheless, we note that if the stellar masses have not changed, then Figure 8 suggests that at $\log_{10}(M_*/M_\odot) > 11.5$, the sizes have increased by a factor of 1.5, and the velocity dispersions have decreased by a factor of 1.15, between $z = 0.27$ and $z = 0.09$. In addition, the dependence of the size and (especially) velocity dispersion of BCGs on formation time (at a given M_*) predicted by Fan et al. ($\Delta \log_{10} R_e > 0.2$ and $\Delta \log_{10} \sigma > 0.1$) is significantly larger than what we observe in Figure 8 (compare dashed with solid curves for a given redshift).

It is interesting to contrast our findings here with the

trends with age for the bulk of the early-type population with $L_r < 10^{11} L_\odot$ (Shankar & Bernardi 2009). In this case, scaling the $R_e - L$ relation by an age-dependent M_*/L ratio, and assuming no change in size, results in better agreement with the actual $R_e - M_*$ relation than we see for our BCGs. However, although the $\sigma - M_*$ relation shows more age dependence than the BCGs, this dependence is weak, suggesting that the formation was not monolithic (but the evidence is less compelling).

These results (i.e. the evolution in size and velocity dispersion at small lookback times, and the weak dependence on formation time of the $\sigma - L$ relation) are more consistent with models which assume that galaxies formed from predominantly dissipationless mergers (Malumuth & Kirshner 1985; Robertson et al. 2006; Boylan-Kolchin et al. 2006; Hopkins et al. 2008). In such models, the stars formed in gas rich mergers at high redshift (explaining the small sizes at early times), but were assembled into BCGs at later times by gas-poor, dissipationless mergers. In these models, the stellar masses, the sizes and the velocity dispersions can evolve, and *the question arises as to whether the mergers were major* (approximately equal size pieces) *or minor*. *Our results suggest that the recent mergers for BCGs were minor*. This is because equal mass mergers have the growth in stellar mass approximately the same as the growth in size, with little change in velocity dispersion (Ciotti 2008). However, our Figure 8 shows that the velocity dispersion decreases.

If the mergers are minor, and the mass increases by a factor of $(1+f)$ in each merger, where $f \ll 1$, then the size increases by $(1+2f)$ and σ^2 decreases by $(1-f)$ in each merger. In this case, a given change in size implies a smaller change in mass than if the changes were caused by a major merger. In this case, we can estimate a required change in mass and size by sliding the $R_e - M_*$ relation at $z = 0.27$ upwards and to the right until it sits above the $z \sim 0.1$ relation: this suggests that $f \approx 0.4$. The predicted evolution in the $\sigma - M_*$ relation can now be compared with that observed; while it is in the right sense, it is a little too strong. The problem can be alleviated slightly if we account for the fact that the stellar mass estimates at low redshift are slightly smaller than they should be, because of mass losses associated with stellar evolution. If so, the implied growth in mass agrees well with that expected in the hierarchical models (De Lucia et al. 2006; Almeida et al. 2007).

We note that a 0.4:1 merger is not what we would call minor; we are supposing that the mass increase of 40% was due to a sequence of minor mergers (e.g. four mergers each adding $\sim 10\%$ to the mass and increasing the size by $\sim 20\%$).

In this context, it is also interesting that motion along an $R_e \propto M_*$ line (major mergers) cannot bring the superdense galaxies recently seen at $z \sim 2$ onto the $z \sim 0$ $R_e - M_*$ relation. However, minor mergers (motion along a line of slope 2 in the $\log(R) - \log(M_*)$ plane) may bring them onto the local relation traced by BCGs. The objects at $z \sim 2$ have large M_* even by $z \sim 0$ standards, so it is not implausible that they are the progenitors of today’s BCGs. This requires mass growth factors of order 4 or 5 (0.6 dex), coupled with an increase in size by a factor of order 10. This is consistent with our estimate of the observed BCG size evolution $(1+z)^{0.85(M_r+21)}$: setting $M_r \sim -23.5$ and $z = 2$ we get an evolution of a factor of ~ 10 .

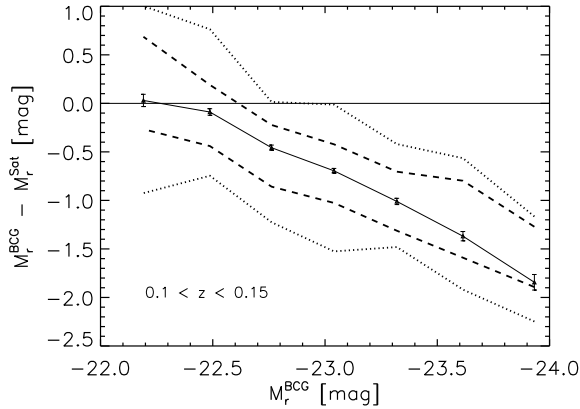


Figure 14. Difference between the luminosity of a satellite galaxy and that of its BCG, as a function of BCG luminosity.

Recent results support our conclusion that minor mergers are important. Hopkins et al. (2008) suggest that if mergers are major, then the fraction of superdense massive galaxies which survived intact since their formation at $z > 2$ could reach 1 – 10%. However, Trujillo et al. (2009) show that the actual number density of superdense galaxies at $z \sim 0$ is much smaller. Minor mergers must account for the difference.

We also compared the ages and sizes of our early-type BCGs with other cluster galaxies (satellites). BCGs are larger than early-type cluster galaxies of similar luminosity or stellar mass at the same redshift (Figure 10). Although satellites and BCGs trace the same weak age- L or age- M_* relation (Figure 12), this can be understood by noting that BCGs are typically about 1 Gyr older than the satellites in their group (Figure 13), and they are about 0.5 mags more luminous (Figure 2).

The mean satellite luminosity is approximately independent of BCG luminosity – a prediction (Skibba et al. 2006) which has recently been confirmed from measurements in other group catalogs (Skibba et al. 2007). Figure 14 shows that this remains true if both BCGs and satellites are required to be early-types. Skibba & Sheth (2008) went on to suggest that satellite colors should also be much weaker functions of group mass than are the colors of centrals, and Skibba (2009) showed that this was indeed the case. Since color is an indicator of M_*/L , and satellite L is almost independent of group mass, M_* should be similarly independent. This prediction has now been confirmed: van den Bosch et al. (2008) find that M_* for satellites changes by a factor of only 2 over a range where group mass changes by a factor of 100. For similar reasons, one expects only a small increase of mean satellite age with BCG luminosity; this is qualitatively consistent with the constant age offset between satellites and BCGs in our Figure 13, and the weak age-luminosity relation for BCGs in our Figure 12.

ACKNOWLEDGMENTS

M.B. is grateful for support provided by NASA grant LTSA-NNG06GC19G. She also thanks Francesco Shankar and Ravi Sheth for helpful conversations.

Funding for the Sloan Digital Sky Survey (SDSS) and SDSS-II Archive has been provided by the Alfred P. Sloan Foundation, the Participating Institutions, the National Science Foundation, the U.S. Department of Energy, the National Aeronautics and Space Administration, the Japanese Monbukagakusho, and the Max Planck Society, and the Higher Education Funding Council for England. The SDSS Web site is <http://www.sdss.org/>.

The SDSS is managed by the Astrophysical Research Consortium (ARC) for the Participating Institutions. The Participating Institutions are the American Museum of Natural History, Astrophysical Institute Potsdam, University of Basel, University of Cambridge, Case Western Reserve University, The University of Chicago, Drexel University, Fermilab, the Institute for Advanced Study, the Japan Participation Group, The Johns Hopkins University, the Joint Institute for Nuclear Astrophysics, the Kavli Institute for Particle Astrophysics and Cosmology, the Korean Scientist Group, the Chinese Academy of Sciences (LAM-OST), Los Alamos National Laboratory, the Max-Planck-Institute for Astronomy (MPIA), the Max-Planck-Institute for Astrophysics (MPA), New Mexico State University, Ohio State University, University of Pittsburgh, University of Portsmouth, Princeton University, the United States Naval Observatory, and the University of Washington.

REFERENCES

- Abbas U., Sheth R. K. 2007, MNRAS, 378, 641
- Adelman-McCarthy, J. K., et al. 2008, ApJS, 175, 297
- Almeida, C., Baugh, C. M. & Lacey, C. G., 2007, MNRAS, 376, 1711
- Barnes, J. E., Hernquist, L., 1991, ApJ, 370, 65
- Becker, M. R. et al. 2007, ApJ, 669, 905
- Bernardi, M., et al. 2003, AJ, 125, 1849
- Bernardi, M., Hyde, J. B., Sheth, R. K., Miller, C. J., & Nichol, R. C. 2007, AJ, 133, 1741
- Bernardi, M., Hyde, J. B., Fritz, A., Sheth, R. K., Gebhardt, K., & Nichol, R. C. 2008, MNRAS, 391, 1191
- Boylan-Kolchin, M., Ma, C. P., & Quataert, E. 2006, MNRAS, 369, 1081
- Buitrago, F., Trujillo, I., Conselice, C. J., Bouwens, R. J., Dickinson, M., & Yan, H. 2008, ApJL, submitted (arXiv:0807.4141)
- Chapman, S. C., et al. 2008, ApJ, in press (arXiv:0807.3674)
- Cimatti, A., et al. 2008, A&A, 482, 21
- Ciotti, L. 2008, La Rivista del Nuovo Cimento, in press (arXiv:0808.1349)
- Damen, M., Labbe, I., Franx, M., van Dokkum, P. G., Taylor, E. N., & Gawiser, E. J. 2008, ApJ, in press (arXiv:0809.1426)
- De Lucia G., et al., 2006, MNRAS, 366, 499
- Fall, S. M., & Efstathiou, G., 1980, MNRAS, 193, 189
- Fan I., Lapi A., De Zotti G., Danese L., 2008, ApJL, submitted (arXiv:0809.4574)
- Franx, M., van Dokkum, P. G., Foerster Schreiber, N. M., Wuyts, S., Labbe, I., Toft, S. 2008, ApJ, in press (arXiv:0808.2642)
- Gallazzi, A., Charlot, S., Brinchmann, J., White, S. D. M., Tremonti, C. A. 2005, MNRAS, 362, 41
- Gunn J., Gott J. R., 1972, ApJ, 176, 1

Hopkins, P. F., Lauer, T. R., Cox, T. J., Hernquist, L. & Kormendy, J. 2008, ApJ, submitted (arXiv:0806.2325)
 Hyde J. B. & Bernardi M. 2009, MNRAS, in press (arXiv:0810.4922)
 Johnston D. E., et al., ApJ, submitted, arXiv:0709.1159
 Koester, B. P. et al. 2007, ApJ, 660, 239
 Lauer, T. R., et al. 2007, ApJ, 662, 808
 Liu, F. S., Xia, X. Y., Mao, Shude, Wu, Hong & Deng, Z. G. 2008, MNRAS, 385, 23
 Malumuth E. M. & Kirshner, R. P. 1981, ApJ, 251, 508
 —. 1985, ApJ, 291, 8
 Meneux, B. et al. 2008, A&A, 478, 299
 Miller C., et al., 2005, AJ, 130, 968
 Nelson A. E., Simard L., Zaritsky D., Dalcanton J. J., Gonzalez A. H., 2002, ApJ, 567, 144
 Oegerle W. R. & Hoessel J. G. 1991, ApJ, 375, 15
 Ostriker J., Hausman M. A., 1977, ApJ, 217, L125
 Robertson, B., Cox, T. J., Hernquist, L., Franx, M., Hopkins, P. F., Martini, P., & Springel, V. 2006, ApJ, 641, 21
 Roche N., Eales S., Rawlings S., 1998, MNRAS, 297, 405
 Saracco, P., Longhetti, M., & Andreon, S. 2008, MNRAS, in press (arXiv:0810.2795)
 Shankar, F. Bernardi, M., 2009, ApJ, submitted
 Shankar, F., Marulli, F., Bernardi, M., Dai, X., Hyde, J., Sheth, R. K., 2009, MNRAS, submitted
 Skibba R. A., Sheth R. K., Connolly A. J., Scranton R., 2006, MNRAS, 369, 68
 Skibba R. A., Sheth R. K., Martino M. C., 2007, MNRAS, 382, 1940
 Skibba R. A., Sheth R. K., 2008, MNRAS, in press (arXiv:0805.0310)
 Skibba R. A., 2009, MNRAS, in press (arXiv:0805.1233)
 Tacconi, L. J., et al. 2008, ApJ, 680, 246
 Toomre, A., & Toomre, J. 1972, ApJ, 178, 623
 Tran K.-V. H., Moustakas J., Gonzalez A. H., Bai L., Zaritsky D., Kautsch S. J., 2008, ApJ, 683, L17
 Trujillo, I., et al. 2006, MNRAS, 373, 36
 Trujillo, I., et al. 2009, ApJL, in press (arXiv:0901.1032)
 van den Bosch, F. et al. MNRAS, 2008, 387, 79
 van der Wel, A., Holden, B. P., Zirm, A. W., Franx, M., Rettura, A., Illingworth, G. D., & Ford, H. C. 2008, ApJ, in press (arXiv:0808.0077)
 van Dokkum, P. G. et al. 2008, ApJL, 677, 5
 Vikhlinin A., Burenin R. A., Ebeling H., Forman W. R., Hornstrup A., Jones C., Kravtsov A. V., Murray S. S., Nagai D., Quintana H., Voevodkin, A., 2008, ApJ, in press (arXiv:0805.2207)
 von der Linden, A., Best, P. N., Kauffmann, G. & White, S. D. M. 2007, MNRAS, 379, 867
 Wake D., et al., 2008, MNRAS, 387, 1045
 Weinmann, S. M., Kauffmann, G., van den Bosch, F. C., Pasquali, A., McIntosh, D. H., Mo, H., Yang, X., & Guo, Y. 2008, MNRAS, submitted (arXiv:0809.2283)
 Whiley I. M., et al., 2008, MNRAS, 387, 1253
 White M., Zheng Z., Brown M. J. I., Dey A., Jannuzi B. T. 2007, ApJ, 655, L69
 Younger, J. D., et al. 2008, ApJ, in press (arXiv:0807.2243)

APPENDIX A: EFFECT OF THE MAGNITUDE LIMIT

The SDSS is magnitude limited. As a result, care must be taken when interpreting redshift-dependent trends. In general, accounting for the selection effect is only straightforward for correlations with luminosity; correlations with stellar mass may be strongly affected – even though M_* and L are tightly correlated. Things are even more complicated if one wishes to study age related trends, since the errors on the age estimates are correlated with those on M_* , and these may be substantial.

A1 Correlations with M_*

To illustrate, the panel on the left of Figure A1 shows the $M_* - L$ relation in a number of redshift bins; there is no trend with redshift. The standard way of accounting for the magnitude limit is to weight each galaxy by the inverse of the volume $V_{\max}(L)$, over which it could have been seen. For the $M_* - L$ relation, this weighting does not matter, as all galaxies in a given L bin have almost the same weight (the weighting matters very much for the $L - M_*$ relation!). The panel on the right shows the $L - M_*$ relation in these same bins, when objects have been weighted by V_{\max}^{-1} : notice how the relation flattens out to constant L at small M_* . The mass scale on which this bias appears depends on redshift, and is purely a consequence of the SDSS magnitude limit – the V_{\max} -weighting does not solve this problem.

Figure A2 illustrates that this can have a dramatic effect on the $R_e - M_*$ relation if it is measured in a narrow redshift bin. The panel on the left shows the $R_e - L$ relation in the same sequence of narrow redshift bins as before. At small L , the $R_e - L$ relation is the same in all the redshift bins; at high L where there is significant curvature in the relation, there is some evidence for evolution. In contrast, the $R_e - M_*$ relation appears to evolve dramatically, particularly at small M_* . It is easy to see that this is a selection effect, and that it produces dramatic effects even though L and M_* are tightly correlated. Consider objects in a given narrow redshift bin. Because of the magnitude limit, objects which scatter to lower L for their M_* will be excluded from the sample. The observed sample will contain objects with large L for their M_* ; since L and M_* are strongly correlated, this will be more dramatic at small M_* ; since size and L are strongly correlated, the exclusion of small L objects biases the sample to large R at small M_* .

Since M_*/L increases with age, the effect of the magnitude limit is particularly pernicious for studies which include both M_* and the age. This is shown in Figure A3. The left hand panel shows that t_{form} , the lookback time from the present to when the stars formed, increases slightly with luminosity. The right hand panel shows the correlation when L is replaced with M_* . For M_* smaller than $10^{11} M_\odot$ the relation for the bulk of the population is changed dramatically. This is because, to make the plot on the right, we have shifted each object in the panel on the left by M_*/L . However, because we have restricted to a narrow bin in z , M_*/L increases with t_{form} , so the shift is larger for large t_{form} . Now, at small M_* , the objects with large M_*/L fell outside the magnitude limit of the survey ($M_r < -21$), so they are missing from the $t_{\text{form}} - M_*$ correlation. Since large

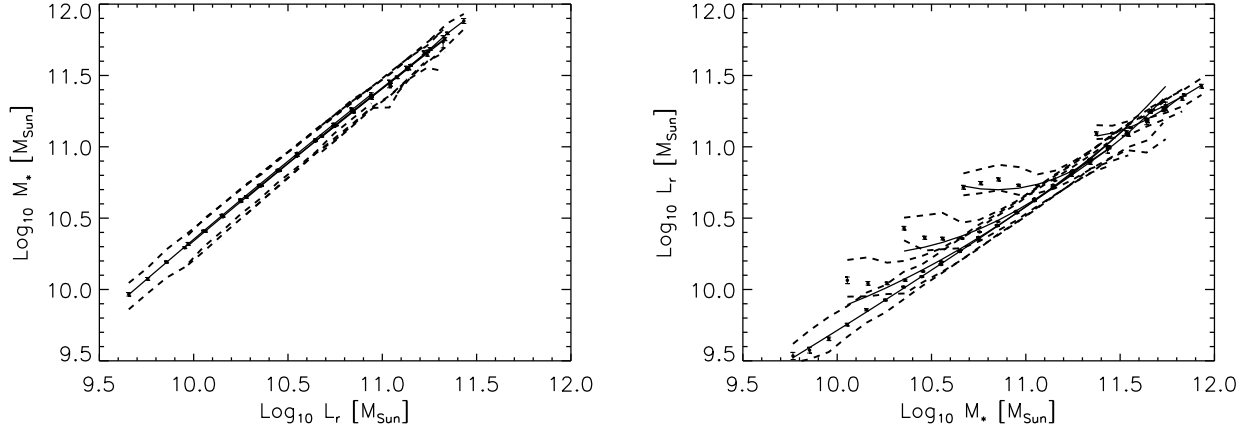


Figure A1. Correlation between stellar mass and luminosity (left) and luminosity and stellar mass (right) in a number of narrow redshift bins. The flattening at (redshift dependent) small M_* in the panel on the right is a selection effect which is due to the magnitude limit of the SDSS.

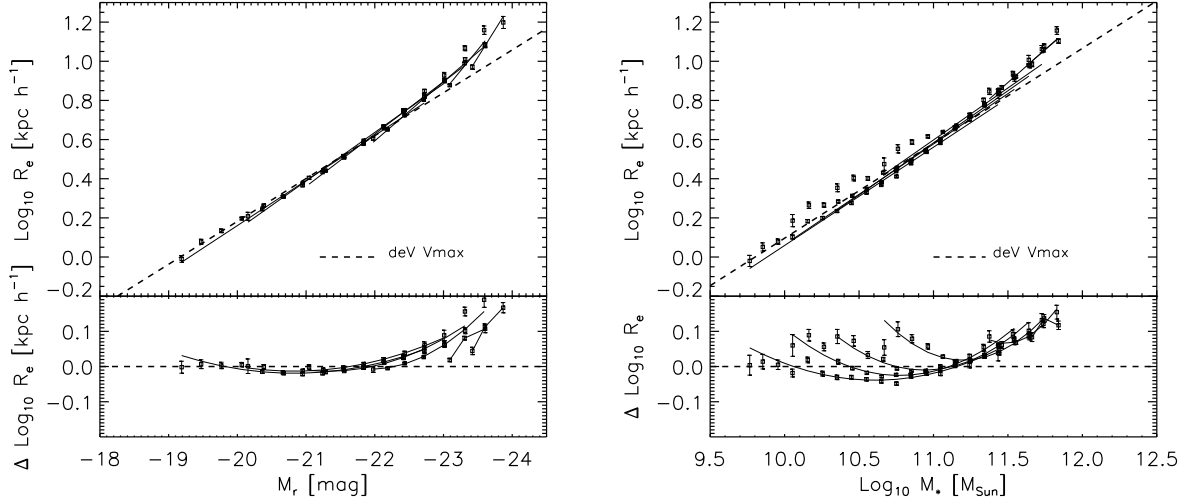


Figure A2. Correlation between size and luminosity (left) and stellar mass (right) in a number of narrow redshift bins. The correlation with luminosity curves upwards at high luminosities; at low luminosities, the relation is not curved, and is independent of redshift. The strongly redshift-dependent curvature at low stellar masses in the panel on the right is a selection effect which is due to the magnitude limit of the SDSS.

M_*/L means large t_{form} , the correlation between t_{form} and M_* curves sharply downwards as a result. We emphasize that this curvature is a selection effect. The satellites and BCGs are far enough from the limiting magnitude that they are less affected by this bias.

A2 Correlations with age and M_*

The main text studies the $R_e - L$ and $R_e - M_*$ correlations as a function of the formation time and the age of the stellar population. However, because the age and M_* estimates have significant uncertainties, and they are correlated, it is important to use ages that are output from the same models which estimate M_* .

Although we cannot actually plot the error in the age versus the error in M_*/L , we expect they will be correlated because, for older stellar populations, $M_*/L \propto t^{0.75}$ or so,

where t is the age of the population. As a result a galaxy that is incorrectly assigned a small age will also be assigned a small M_*/L ratio. In addition, if the uncertainty on the age is small then the uncertainty on M_*/L , and hence M_* will also be small. This explains the trends shown in the bottom panels of Figure A4 (note that these do not show the correlated errors themselves – they show that when one quantity has a large error bar, then so does the other). Notice that when the estimated age is small, then the uncertainties on the age increase dramatically; this increases the uncertainty on M_* as well.

Correlated errors in age and M_*/L complicate analyses of how galaxy structure correlates with formation time and age. To illustrate, Figure A5 shows M_*/L as a function of L and M_* for a number of bins in formation time. The panel on the left is not very surprising – galaxies which formed longer ago have larger M_*/L ratios – although it ap-

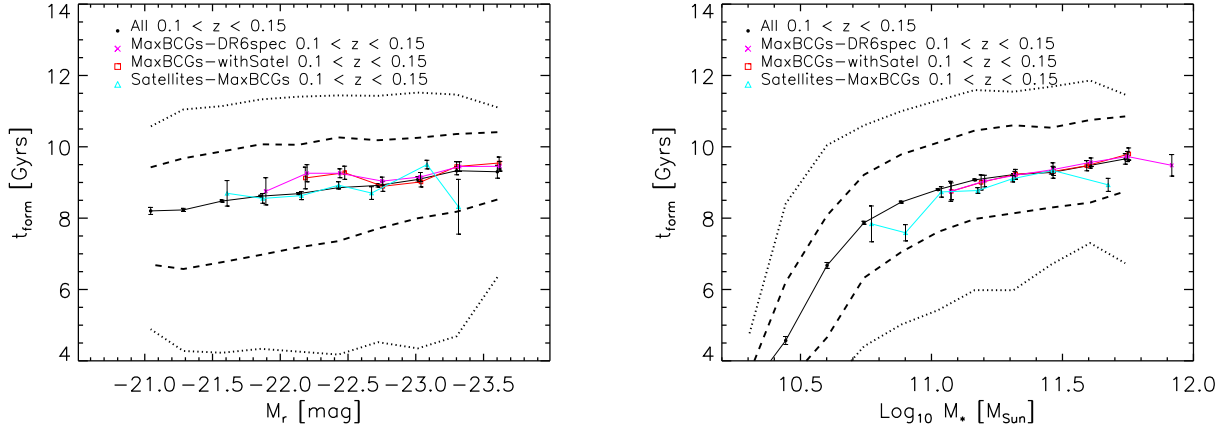


Figure A3. Correlation between (lookback time to) formation and luminosity (left), and stellar mass (right), for BCGs (squares and crosses), satellites (triangles), and the bulk of the population (filled circles with error bars), over the redshift range $0.1 < z < 0.15$. The drop at small M_* is a selection effect.

pears that there may be something amiss in the bin with the most recent formation times. The offset from one bin to another is consistent with the expected fading of an old stellar population: $M_*/L \propto t^{0.75}$ or so, where t is the age of the population. Figure A6 shows this explicitly: when the luminosity has been corrected for this age effect, then the different formation time bins overlap.

It is worth noting that using age estimates from a different algorithm than the one which provided the M_*/L estimates results in qualitatively similar behaviour to that shown in the lefthand panel of Figure A5, except that the offset between the different formation time bins is smaller. This is because, if this is done, then the correlated nature of the age and M_*/L errors is missing. As a result, it would be possible for an object to be assigned a younger age than its true one, as well as a larger M_*/L ratio than its true one, and so objects assigned recent formation times would have larger M_*/L ratios on average, and objects assigned older formation times have smaller M_*/L ratios, than when the errors in age and M_*/L are correlated.

Unfortunately, the presence of correlated errors produces spurious features in the right hand panel of Figure A5. In this case, errors in M_*/L move objects along lines that slope upwards and to the right. But if an object scatters downwards and to the left along such a line (of constant L), it is also assigned a younger age, and so it contributes to a more recent formation time bin. If there are, in fact, no real galaxies having large M_* but recent formation times, then the correlated errors will have produced such a population. Since the uncertainties are largest for the youngest galaxies, we believe that it is this effect which causes the sharp upturn in the lowest two formation time bins.

A better procedure, if only the age or only M_* is known, is to assume that $\partial \log(M_*/L)/\partial \log t = 0.75$, and to use this to correct luminosities for age effects. Thus, when we use L^{corr} as a proxy for M_* , we obtain the correct spread in ages at fixed L (solid lines in Figure A5), and we find $M_*/L^{\text{corr}} \approx \text{constant}$ (Figure A6).

APPENDIX B: COMPARISON WITH PREVIOUS WORK AT $Z < 0.1$

The size-luminosity relation for BCGs has been the subject of much recent interest (Lauer et al. 2007; Bernardi et al. 2007; von der Linden et al. 2007; Liu et al. 2008). Whereas most authors agree that early-type BCGs are very different from the bulk of the population, von der Linden et al. (2007) find substantially smaller differences. This is almost certainly because von der Linden et al. use Petrosian-based quantities, and these have been compromised by seeing (Hyde & Bernardi 2009).

However, the $R-L$ scaling relation from Bernardi et al. (2007) differs slightly from that found in the main text above. Figure B1 compares the relation for C4 BCGs reported by Bernardi et al. (2007) (long dashed line), with our present determination (symbols and dashed-triple-dot line) for the same BCGs; the Bernardi et al. sizes are slightly smaller, and the scaling relation is slightly shallower. We have traced this to the fact that, although both sizes come from 2d fits to the surface brightness profile, our size is an effective circular size ($R = \sqrt{ab}$), whereas Bernardi et al. inadvertently show the minor axis b , even though they state that they show \sqrt{ab} (a result of correcting the long axis a by two powers of $\sqrt{b/a}$ rather than just one). Correcting for this effect makes their relation the same as ours. For completeness, this relation is

$$\log_{10} \left(\frac{R_e}{\text{kpc}} \right) = 0.158 - 0.423 (M_r + 21). \quad (\text{B1})$$

However, Figure B2 compares the scaling we find for the C4 BCGs with that reported by Lauer et al. (2007). Although both relations are clearly more like one another than like the bulk of the population, there are significant differences. Some of this is due to systematic differences between the two reductions, and, in light of the results in the main text, some may be due to evolution: the Lauer et al. sample is at even lower redshifts than our C4 sample. This, of course, does not explain the offset at smaller luminosities.

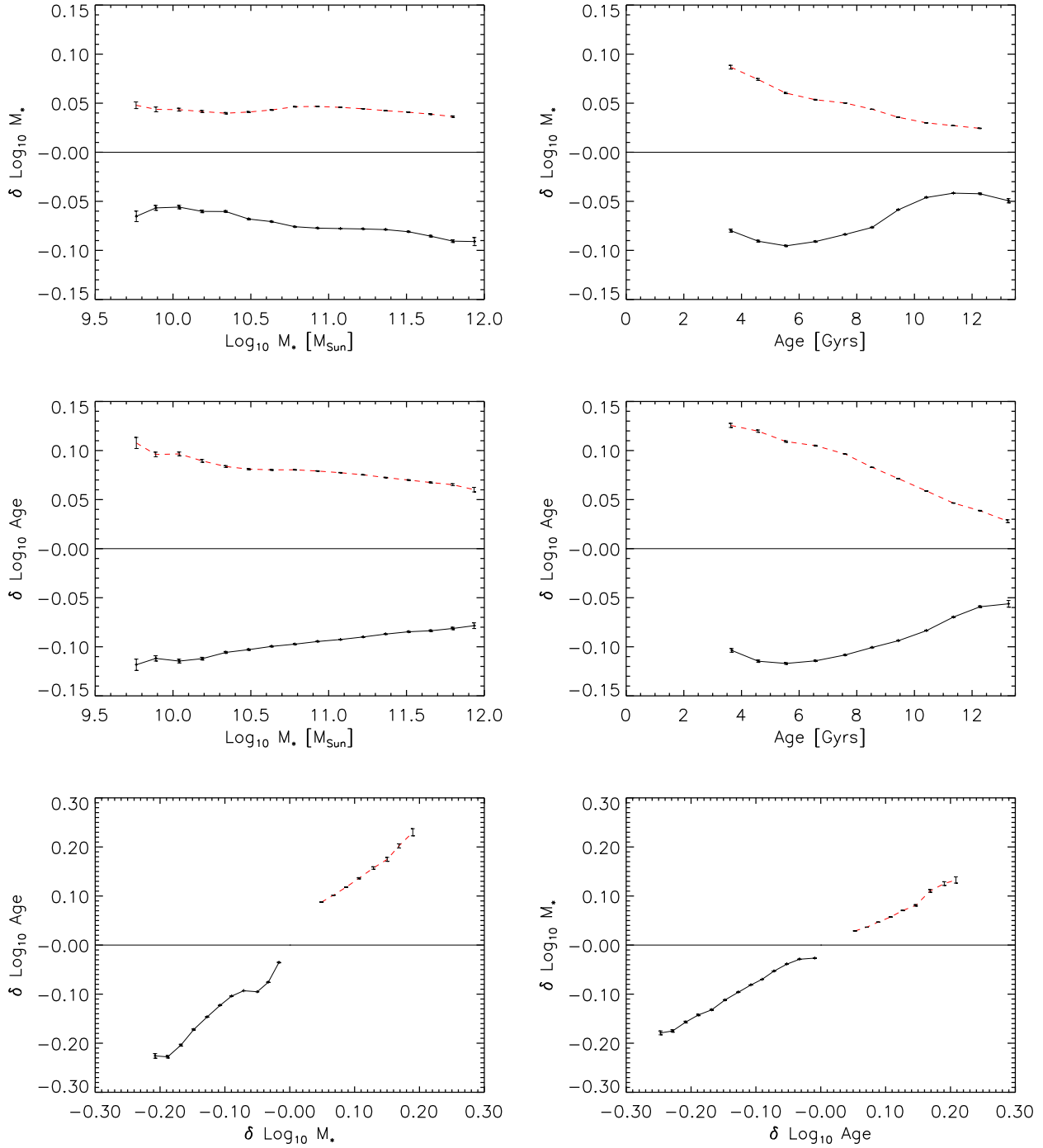


Figure A4. Uncertainties on estimated ages and stellar masses. Dashed line shows the difference between the 84th percentile of likelihood distribution of the measured age or stellar mass and the 50th percentile; solid line shows the difference between the 16th and 50th percentile. The error on $\log_{10} M_*$ develops a tail which extends to small masses when M_* is large (top left), and it increases dramatically for ages below 9 Gyrs (top right). The error on the age increases at small M_* (middle left) and age (middle right). When the error on M_* is large, so is the error on the age (bottom left), and vice versa (bottom right).

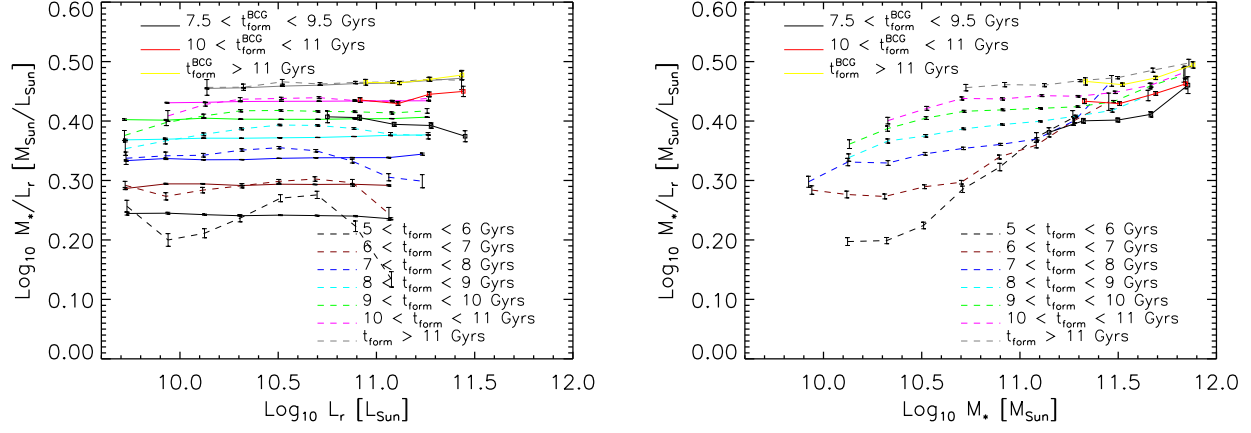


Figure A5. Stellar mass to light ratio as a function of luminosity (left), and M_* (right); the slight curvature at the small M_* for each bin in t_{form} is due to the same selection effect as in Figure A3. The sudden increase in M_*/L at larger M_* (right panel) and decrease in M_*/L at larger L (left panel) for the younger galaxies is due to correlated errors. Symbols connected by solid and dashed lines show the MaxBCGs-DR6spec sample and bulk of the early-type population, respectively. Horizontal solid lines in left panel show the expected M_*/L given the age: $d \log(M_*/L)/d \log t = 0.75$.

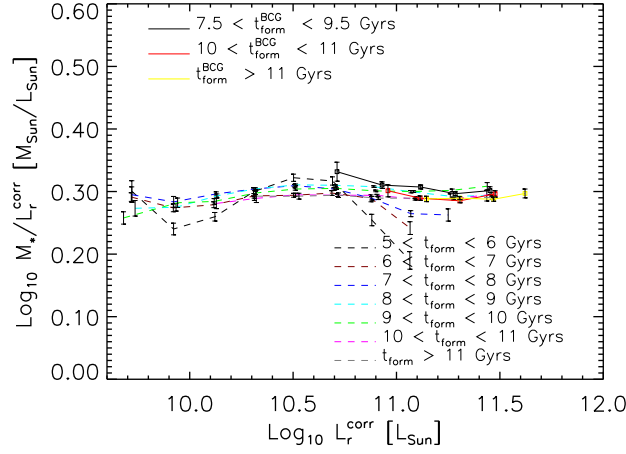


Figure A6. Stellar mass to light ratio as a function of luminosity, where the luminosity has been corrected for age effects assuming $d \log(M_*/L)/d \log t = 0.75$. Here, we corrected the luminosity to a population 6.5 Gyr old, i.e. $\text{log}_{10} L_r^{\text{corr}} = \text{log}_{10} L_r + 0.75(\text{log}_{10} t - \text{log}_{10} 6.5)$. Lines as in Figure A5.

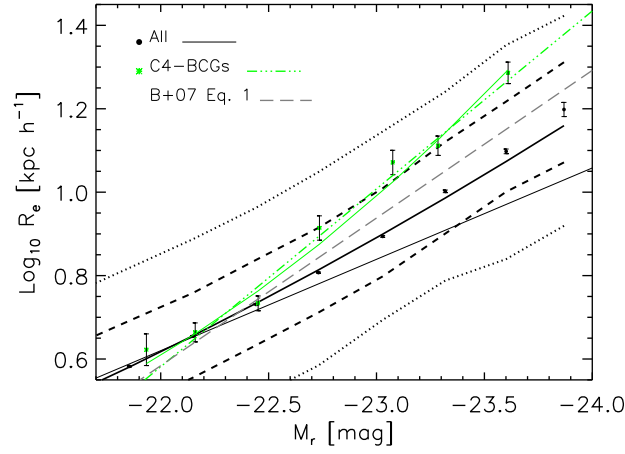


Figure B1. Comparison of our measurement of the size-luminosity relation in the C4 sample with that reported by Bernardi et al. (2007). Our sizes are larger, and the scaling relation steeper, because we set $R = \sqrt{ab}$, where a and b are the major and minor axis lengths; Bernardi et al. inadvertently set $R = b$.

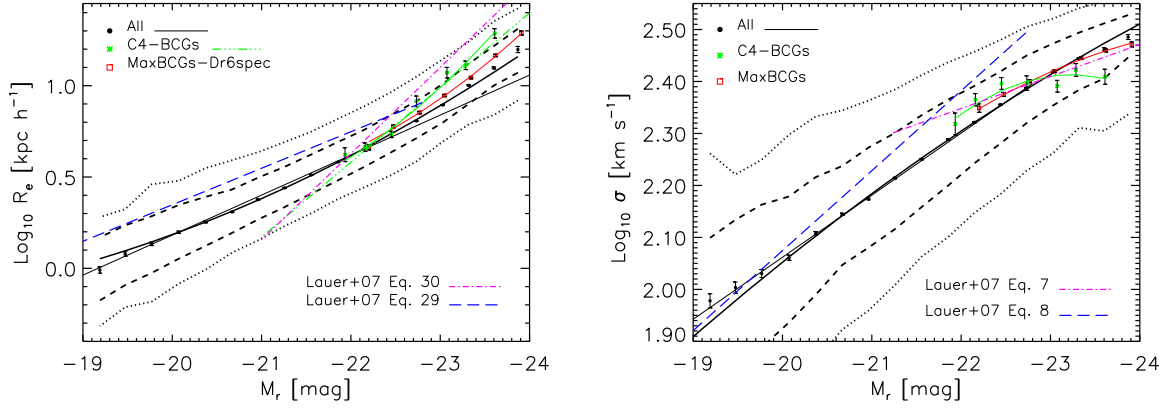


Figure B2. Comparison of the size-luminosity and velocity dispersion-luminosity relations (top and bottom panels) in our data with that reported by Lauer et al. (2007).